WFIRST Technical Report
Doc #: WFIRST-STScI-TR1603
Rev: A
Date: March 3, 2016

Slitless Grism Spectroscopy with WFIRST: Pointing Reconstruction from Dispersed Images

William V. Dixon

Abstract

The spectroscopic component of the WFIRST High-Latitude Survey will determine the redshift of distant galaxies with an accuracy $\sigma_z/(1+z) \leq 0.001$. To achieve this goal, the spacecraft pointing must be known to better than 21 mas. The baseline operational plan is to derive this information directly from the measured positions of bright stellar spectra in the dispersed images. An initial analysis suggested that this measurement would be difficult; however, a new set of effective-area curves for the WFIRST grisms reveals that the filter bandpass edges of the WFIRST grisms are sufficiently sharp (< 1%) that reconstruction of the spacecraft pointing with the required accuracy will be straightforward.

1. Introduction

When wide-field slitless spectroscopy (WFSS) is performed using *HST*, a direct (undispersed) image is always obtained in the same visit as the dispersed image. A source catalog listing the measured position (*X* and *Y* on the detector) of each object in the direct image is used to compute the trace and wavelength solution of its spectrum in the dispersed image. These relationships are well calibrated, and this technique is quite successful (e.g., Brammer et al. 2012). As currently envisioned (Cassertano et al. 2015), the imaging and spectroscopic components of the WFIRST High-Latitude Survey will be conducted independently. As a result, a dispersed image will not have a corresponding direct image from which to derive its source catalog.

The SDT final report (Spergel et al. 2015) assumes that the pointing of each dispersed image in the spectroscopic survey can be determined *a posteriori* from the cross-dispersion and bandpass cutoff edges of the spectra of bright stars in the field. If the pointing can be reconstructed precisely, then the object catalog produced by the imaging survey can be mapped onto the detector, and a source catalog constructed. The redshift accuracy required of the spectroscopic survey is $\sigma_z/(1+z) \leq 0.001$. Kruk (2015) has derived an error budget for the redshift measurement; it allows for a statistical uncertainty of 21 mas in the pointing knowledge derived from bright stars in the field, which

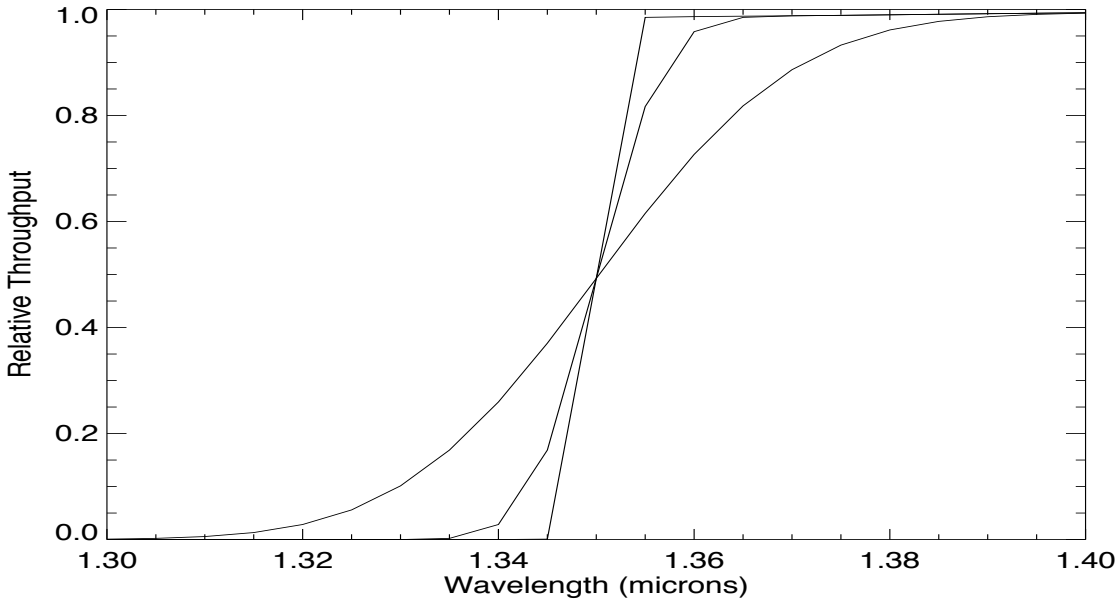

Figure 1. Grism throughput curves with 10%-90% transmission widths of 0.3%, 1%, and 3% of the midpoint wavelength.

corresponds to a 2 Å uncertainty in the wavelength of the bandpass cutoff. (This value is added in quadrature to the other uncertainties in the error budget.) In this report, we investigate whether an accuracy of 2 Å is achievable.

2. Wavelength Calibration Uncertainties Using Filter Edges

Measuring the positions of spectra in the cross-dispersion direction is straightforward, but measuring the bandpass cutoff edges is more challenging, because they depend on the shape of the filter throughput curves, knowledge of the source spectrum, and the signal-to-noise ratio of the observed spectra. We consider only measurements of the bandpass cutoff edges.

2a. Initial Throughput Curves

We first used an early set of effective-area curves for which the filter bandpass edges are relatively broad: the 10%-90% transmission width is 3% of the midpoint wavelength (Figure 1). The vendors promise much narrower edges, and the first filter samples have transmission widths of less than 1% for both the blue and red filter edges. Though the following results are thus somewhat dated, they are instructive, as they demonstrate the effects at play.

Bandpass edges are measured by computing the wavelength shift between a set of “observed” spectra and a reference spectrum (Figure 2). We consider

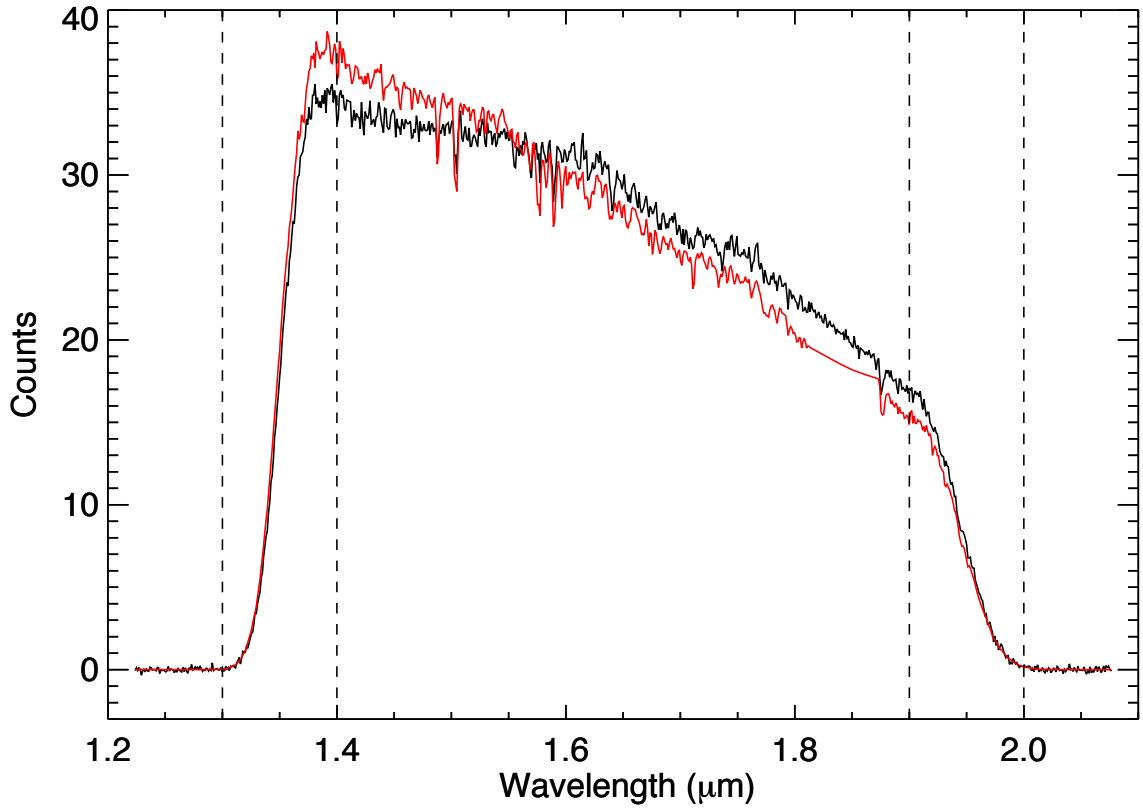

Figure 2. Comparison of observed and reference spectra. Reference spectrum (red) is a K0 dwarf, modeled without noise. Observed spectrum (black) is a K0 giant. Only regions between 1.3 and 1.4 μm (blue edge) and 1.9 and 2.0 μm (red edge) are considered.

only wavelengths between 1.3 and 1.4 μm (the blue edge) and 1.9 and 2.0 μm (the red edge) and shifts between -30 and +30 Å with a step size of 0.25 Å. At each step, we fit the reference spectrum to the data. The scale factor of the reference spectrum is the only free parameter. We perform three fits: the blue edge, the red edge, and the blue+red edges together. In the third case, to account for variations in the spectral slope, the scale factors for the blue and red edges are allowed to vary independently. The best-fit shift is determined by its χ^2 value.

We began by generating synthetic spectra for stars with H-band magnitudes ranging from 16 to 19. We ran 100 spectral models at each magnitude, using a K0V spectrum (HD 145675) from the IRTF Spectral Library (Rayner et al. 2098) to generate both the artificial data and the reference spectrum. The reference spectrum was constructed with all sources of noise turned off. All spectra were generated with aXeSIM and extracted with aXe (Kümmel et al. 2009). Below are listed the mean and standard deviation of the best-fit shift in Ångstroms. While

the mean shift is essentially zero for all magnitudes, the standard deviation exceeds 2 Å for stars fainter than 18th magnitude.

	BLUE EDGE	RED EDGE	BLUE & RED EDGES
mag = 16.0	-0.023 +/- 0.376	0.011 +/- 0.356	-0.019 +/- 0.258
mag = 16.5	-0.036 +/- 0.526	0.037 +/- 0.762	-0.041 +/- 0.373
mag = 17.0	-0.022 +/- 0.644	0.219 +/- 1.298	0.025 +/- 0.517
mag = 17.5	0.091 +/- 1.172	-0.087 +/- 2.043	0.130 +/- 0.827
mag = 18.0	0.110 +/- 1.658	0.104 +/- 2.807	0.162 +/- 1.401
mag = 18.5	-0.048 +/- 2.875	0.513 +/- 3.161	-0.069 +/- 2.471
mag = 19.0	-0.208 +/- 3.006	-0.056 +/- 3.518	-0.295 +/- 2.742

To examine the effects of small differences in the spectral type, we repeated the analysis, using a K0 giant (HD 100006) as the observed spectrum and the K0 dwarf as the reference (Figure 2). Shifts as a function of magnitude are listed below. We find systematic offsets between the two spectra, offsets that differ for the blue and red edges of the filter. The fact that the mean shift decreases for fainter stars reflects the increasing noise in their spectra.

	BLUE EDGE	RED EDGE	BLUE & RED EDGES
mag = 16.0	3.910 +/- 0.577	-1.153 +/- 2.914	3.323 +/- 0.536
mag = 16.5	3.872 +/- 0.675	-1.320 +/- 3.170	3.274 +/- 0.629
mag = 17.0	3.730 +/- 1.082	-1.134 +/- 3.799	3.202 +/- 1.210
mag = 17.5	3.588 +/- 1.994	-0.804 +/- 4.703	3.138 +/- 1.898
mag = 18.0	3.328 +/- 2.837	0.776 +/- 5.690	2.956 +/- 2.852
mag = 18.5	2.248 +/- 4.574	0.096 +/- 10.947	1.860 +/- 4.530
mag = 19.0	0.408 +/- 6.481	2.336 +/- 12.018	1.148 +/- 6.685

What is happening? The “edge of the spectrum” is the product of the filter throughput and the stellar continuum. Changes in the spectral slope can shift it to the blue or red. Spectral features falling near the filter edge can alter its shape. In this case, both effects are at play. On the blue end, the dwarf’s spectrum is considerably steeper than the giant’s. On the red end, the continua are similar, but the dwarf spectrum has more absorption features.

2b. New Filter Throughput Curves

The bandpass cutoff edges of the WFIRST grism will have transmission widths as narrow as 0.7% or 0.8% (J. Kruk 2015, private communication). To more accurately reflect this design, we repeated the analysis using a set of throughput curves with 1% edges (Figure 1).

For this analysis, we developed software that converts model spectra into synthetic observed spectra directly, without employing the machinery of aXe. The program reads a stellar spectrum, scales it to a desired H_{AB} magnitude (computed using the throughput curve of the WFIRST H158 filter), and converts it from units of flux density to e^{-} s^{-1} $pixel^{-1}$ on the WFIRST detector. The program smooths the spectrum to the resolution of WFIRST by convolving it

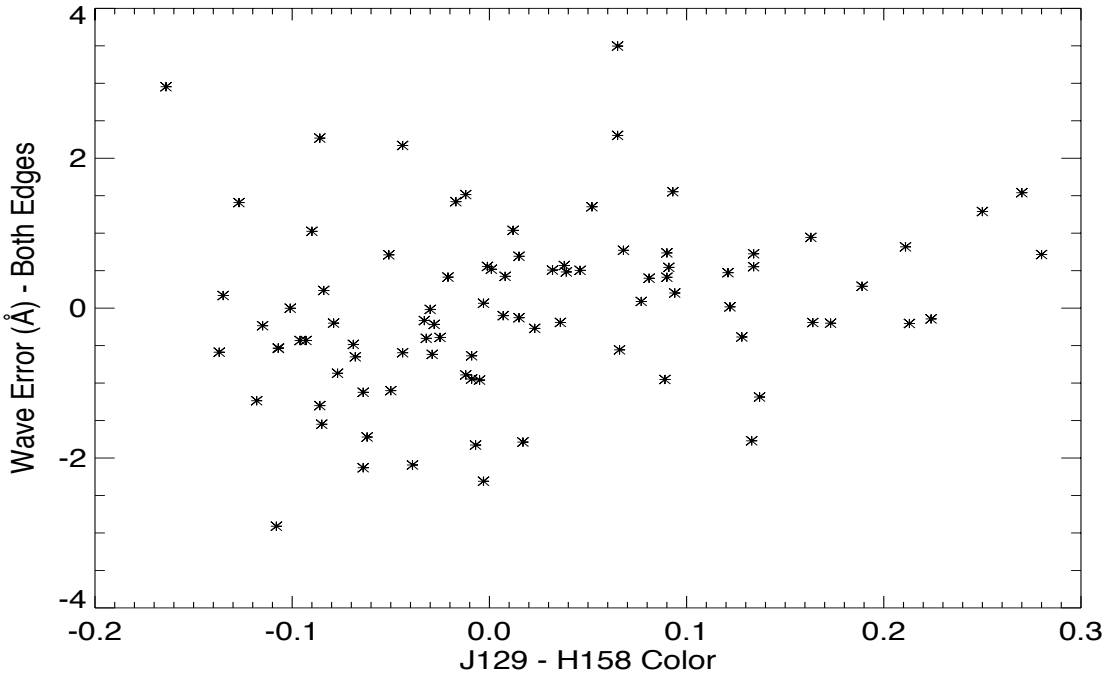

Figure 3. Error in the derived wavelength scale for each of the 89 stars in our sample, plotted as a function of the star's J – K color.

with a Gaussian kernel with FWHM = 2 pixels. It adds dark current (0.824 e^- s^{-1} $pixel^{-1}$), Gaussian noise, and read noise (5.25 e^- $pixel^{-1}$), assuming that the spectrum is spread over four detector pixels in the cross-dispersion direction (a region encompassing 99.7% of the stellar flux). The resulting observed spectrum is compared to a noise-free reference spectrum, which is now the K0 giant (HD 100006). The new program uses 2 Å steps from -50 to +50 Å. Instead of simply accepting the fit that yields the minimum value of χ^2, it fits a parabola to the χ^2 array and adopts the lowest point of the parabola as the best-fit wavelength offset. This two-step process smooths over noise peaks and spectral features, reducing the scatter. The fit is performed three times, considering the blue edge of the spectrum, the red edge, and both edges together. This process is repeated for each of the 89 G and K stars in the IRFT Spectral Library and for H_{AB} magnitudes between 16 and 19.

The following values represent the average offsets in Ångstroms for the 89 stars in our sample. Error bars represent the standard deviation about the mean. We see that, when the red and blue edges of the spectra are fit simultaneously, the mean offset is essentially zero – and the standard deviation less than 2 Å – for all stars 18th magnitude or brighter.

H_AB	BLUE EDGE	RED EDGE	BLUE & RED EDGES
16.0	0.378 +/- 1.786	-1.753 +/- 2.873	0.008 +/- 1.140
16.5	0.326 +/- 1.771	-1.901 +/- 3.045	-0.042 +/- 1.145
17.0	0.390 +/- 1.786	-1.736 +/- 2.906	0.031 +/- 1.190
17.5	0.453 +/- 1.974	-2.078 +/- 3.667	0.083 +/- 1.451
18.0	0.250 +/- 1.924	-1.686 +/- 3.522	-0.056 +/- 1.464
18.5	0.442 +/- 2.610	-1.598 +/- 4.957	0.159 +/- 2.168
19.0	0.267 +/- 2.731	-0.754 +/- 5.940	0.057 +/- 2.308

Using 2MASS data at the North Galactic Pole, Kruk (2015) estimates that there is a 96% probability of finding at least six stars with $15.5 < H_{AB} < 17.5$ in any single WFIRST detector, so the pointing can be determined independently for each image in the survey. Combining the spectra from all 18 detectors will further reduce the pointing uncertainty.

3. Conclusions and Future Work

These results suggest that the spacecraft pointing can be determined directly from the spectra of bright stars ($H_{AB} \leq 18$) in dispersed images obtained for the WFIRST High-Latitude Survey with sufficient accuracy to meet its redshift-accuracy requirements.

The WFIRST data-reduction pipeline will employ algorithms more complex than the simple scheme presented here. For example, faint companions may contaminate the spectra of some bright stars, so a way of identifying and rejecting outliers will be needed. Data from GAIA or ground-based surveys can be used to identify stars with well- or poorly-behaved spectra. The spectral resolution of WFIRST is high enough that the observed spectra of these bright stars could be used to constrain their spectral types. Indeed, a catalog of stellar magnitudes and spectral types (especially for stars fainter than the GAIA sample) would be a useful product of the survey.

Acknowledgements

This work was carried out under contract with the WFIRST Study Office at NASA Goddard Space Flight Center (GSFC), as part of the joint pre-formulation science center studies by the Space Telescope Science Institute (STScI) and the Infrared Processing and Analysis Center (IPAC). The author is grateful to Jeff Kruk and the STScI Slitless Spectroscopy Working Group for discussions and feedback.

References

Brammer, G. B., et al. 2012, ApJS, 200, 13
Cassertano, S., et al. 2015, Slitless Grism Spectroscopy with WFIRST: Observing Modes and Strategies, WFIRST-STScI-TR1506

Kruk, J. 2015, Comments on the Spectrometer Resolution Required for Measurements of Emission Line Redshifts with Accuracy $\sigma_z/(1+z) \leq 0.001$, unpublished
Kümmel, M., Walsh, J. R.; Pirzkal, N., Kuntschner, H., & Pasquali, A. 2009, PASP, 121, 59
Rayner, J. T., Cushing, M. C., & Vacca, W. D. 2009, ApJS, 185, 289
Spergel, D., et al. 2015, WFIRST-AFTA 2015 Report, arXiv/1503.03